Special Issue Article

Journal of PeptideScience

Received: 17 December 2014 Accepted: 17 December 2014 Published online in Wiley Online Library

(wileyonlinelibrary.com) DOI 10.1002/psc.2742

Soft structure formation and cancer cell transport mechanisms of a folic acid–dipeptide conjugate‡

Gagandeep Kaur,[a] Akansha Shukla,[d] Sri Sivakumar[b,c,d] and Sandeep Verma[a,b,c]*

Folic acid (FA) is a low-molecular-weight micronutrient, which plays a critical role in the prevention of birth defects and cancers. It is also essential for biochemical pathways responsible for DNA synthesis and maintenance and for the generation of new red blood cells. Cellular trafficking of FA and folate is based on its high-affinity binding to cognate folate receptor, a protein commonly expressed in several human cancers. Thus, folate conjugates of drugs, plasmids, biosensors, contrast, and radiodiagnostic imaging agents have been used for assisted delivery in folate receptor-positive cancer cells, via endocytosis pathways. This report describes morphologies of soft structures from a fully characterized FA–dipeptide conjugate and detailed mechanistic studies of its cancer cell uptake, as tracked by the inherent fluorescence of the conjugate. Copyright © 2015 European Peptide Society and John Wiley & Sons, Ltd.

Additional supporting information may be found in the online version of this article at the publisher's web site.

Keywords: folic acid; diphenylalanine; self-assembly; cell delivery

Introduction

Folic acid (FA)-conjugated imaging agents and candidate drugs have evoked considerable interest over the years because of their ability to enter cancer cells, through high-affinity interaction with folate receptor (FR) protein. FRs, particularly FRα, exhibit hyperactivity in several cancer cells such as breast, brain, lungs, cervical, and renal carcinomas [1,2] and offer a key entry point supporting active folate intake in cancer cells [3]. Subsequent to FR binding in cancer cells, folate conjugates are transported inside cells via endocytosis [4,5]. Chemical functionalities in FA play key roles in high-affinity FR binding [6], and subsequent to cellular entry of folate conjugates, enzymatic transformations release bioactive molecules inside cells. Increased involvement of FRs in cancer cells makes this strategy very useful for delivery of drugs and bioactives [7–9]. Over a period of time, many such conjugates have entered different stages of clinical studies to deliver chemotherapeutic drugs to target cells [10,11]. However, main impediments of such conjugates, which limit their widespread use, concern lack of conjugate stability and cytotoxicity.

From the standpoint of supramolecular chemistry, FA consists of a heterocyclic pterin skeleton, which affords self-assembled structures belonging to cholesteric and hexagonal mesophases, under mild alkaline conditions [12,13]. Suitably disposed donor-acceptor sites in pterin skeleton drive hydrogen bond-assisted self-recognition event, in a manner analogous to guanine tetramer formation, and it is shown that the presence of monovalent cations imparts stability to cholesteric phases. A recent study demonstrated that a change in monovalent cations resulted in enhanced FA tetramer rigidity, as a result of favorable stacking interactions and tetrad elongation [14,15].

Given our ongoing interest in peptide soft structures [16–25] and bionanoconjugation based on guanine tetrad formation [26], we decided to investigate whether bottom-up approach with FA-containing peptide building blocks will reveal interesting structural features and delivery properties. The design of FA conjugates could be achieved via two different routes: first, by making FA-conjugated peptides, followed by their self-assembly, or through postsynthetic modification of *in situ* assembled peptide nanotubes by FA (Scheme 1) [27]. The former approach offers superior control over gross morphology of soft structures and the possibility of additional chemical modifications to create a multivalent, folate-displaying building block. We decided to employ Phe–Phe dipeptide for the synthesis of a FA-conjugated building block (Scheme 2), as both dipeptide and FA demonstrate remarkable ability to self-assemble in solution [12–15,28–32]. Thus, we envisaged that it would be intriguing to study how ensuing covalent conjugation will affect self-assembly and gross morphology. We also decided to perform cytotoxicity assays and study of possible cell uptake mechanism in different cancer cell lines.

* *Correspondence to: Sandeep Verma, Center for Environmental Sciences and Engineering, Indian Institute of Technology Kanpur, Kanpur 208016, India. E-mail: sverma@iitk.ac.in*

‡ *Invited Article for the Anniversary Issue 2015 of Journal of Peptide Science.*

a *Department of Chemistry, Indian Institute of Technology Kanpur, Kanpur 208016, India*

b *DST Thematic Unit of Excellence on Soft Nanofabrication, Indian Institute of Technology Kanpur, Kanpur 208016, India*

c *Center for Environmental Sciences and Engineering, Indian Institute of Technology Kanpur, Kanpur 208016, India*

d *Department of Chemical Engineering, Material Science Programme, Indian Institute of Technology Kanpur, Kanpur 208016, India*

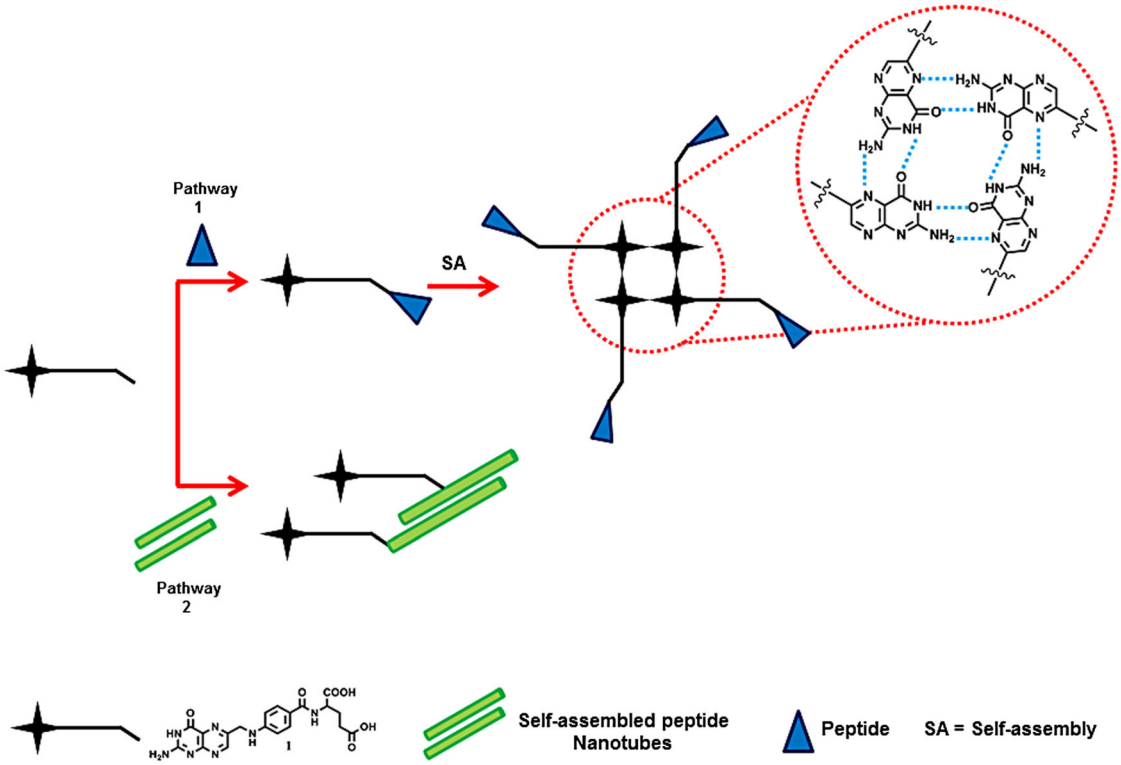

Scheme 1. Two approaches for folic acid and diphenylalanine dipeptide conjugate design (inset: hydrogen-bonded pterin tetrad).

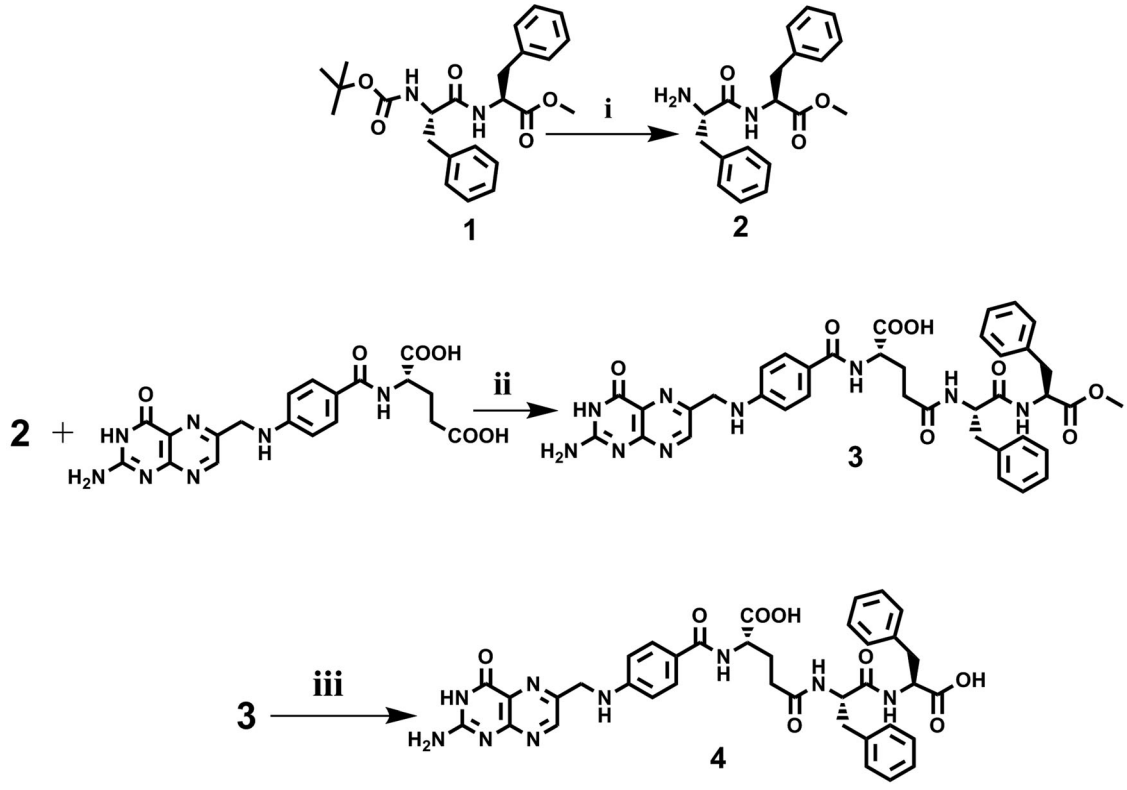

Scheme 2. Synthetic scheme for peptide **4**: (i) 75% TFA–DCM, 4 h, N_2 atmosphere; (ii) N, N′-dicyclohexylcarbodiimide, pyridine, dark; and (iii) 1 N HCl, 6 h.

Journal of PeptideScience

Experimental Section

Chemical Synthesis

Material and methods

N, N′-Dicyclohexylcarbodiimide (DCC), TFA, and L-phenylalanine (Phe) were purchased from SRL, Mumbai, India, and used without further purification. DCM, N,N-dimethylformamide (DMF), pyridine, methanol, and trimethylamine were distilled according to standard procedures prior to use.

Peptide conjugate synthesis

Conjugate **4** was prepared by standard solution phase peptide synthesis. Scheme 2 shows various synthetic steps.

L-Phenylalanine-L-Phenylalanine Methyl Ester Folic Acid Conjugate (3)

Folic acid (250 mg, 556 mmol), **2** (184 mg, 556 mmol), and DCC (128 mg, 623 mmol) were dissolved in DMSO (5 ml) in the presence of dry pyridine (10 μL). The mixture was stirred overnight, in the dark, at room temperature under nitrogen atmosphere. Afterwards, the mixture was diluted with deionized water (10 ml) and centrifuged at 1000 rpm for 30 min to separate insoluble dicyclohexylurea. The supernatant was collected and washed with diethyl ether to give a yellow precipitate, which was filtered and dried. The crude compound was further purified by silica gel column chromatography eluting with methanol-DCM to isolate a pure yellow-colored compound (180 mg, 72% yield). High-resolution mass spectrometry $(M+H)^+$ for $C_{38}H_{40}N_9O_8$: 750.3000 (Calcd.), 750.3000 (Anal.), ^{1}H NMR (500 MHz, d^6-DMSO, TMS, δ ppm): 1.17–1.22 (m, 4H), 1.45–1.75 (m, 4H), 2.46 (s, 3H), 3.31 (s, 2H), 3.45–3.52 (m, 3H), 6.59–7.62 (m, 14H), 7.91 (s, 3H), 8.61 (s, 3H), 9.05 (s, 1H), 11.40 (s, 1H); ^{13}C NMR (125 MHz; d^6-DMSO, δ ppm): 25.7, 34.6, 36.7, 42.4, 46.4, 48.3, 52.2, 52.7, 54.1, 54.9, 111.7, 121.7, 126.7, 127.0, 128.5, 128.7, 129.6, 149.0, 149.2, 151.3, 152.8, 154.4, 158.9, 166.9, 171.9, 172.2, 174.3, 174.4.

L-Phenylalanine-L-Phenylalanine Folic Acid Conjugate (4)

Conjugate **3** (100 mg) was dissolved in 15 ml of 1 N HCl and stirred for 6 h. The residue was filtered and washed with diethyl ether/acetone (70 : 30) to achieve yellow precipitates of **4**, which was filtered and dried (80 mg, 80% yield). High-resolution mass spectrometry $(M-H)^-$ for $C_{37}H_{36}N_9O_8$: 734.2687 (Calcd.), 734.2689 (Anal.), ^{1}H NMR (500 MHZ, d^6-DMSO, TMS, Δ ppm): 1.68–1.80 (m, 4H), 2.03–3.51 (m, 4H), 4.50 (s, 3H), 6.20–7.63 (m, 14H), 7.90–7.96 (m, 1H), 8.21 (m, 2H), 8.45–8.48 (m, 3H), 8.69–8.86 (s, 1H), 9.02 (S, 1H), 10.60 (s, 1H); ^{13}C NMR (125 MHZ; d^6-DMSO, Δ ppm): 25.84, 30.44, 36.06, 39.35, 47.17, 53.07, 57.45, 59.69, 116.51, 132.07, 132.20, 133.23, 133.52, 134.39, 147.16, 148.04, 148.08, 148.08, 148.97, 150.04, 150.21, 158.44, 163.65, 167.56, 167.70.

Field Emission Scanning Electron Microscopy

The 10 μl aliquots of samples (1 mM and 10 μM solutions of conjugates **3** and **4**) were deposited on a silicon wafer (100) and allowed to dry at room temperature. Subsequently, the samples were dried *in vacuo* for 30 min prior to imaging. Samples were gold-coated, and scanning electron microscopy (SEM) images acquired on FEI Quanta 200 microscope (Zeiss Supra 40VP, Jena, Germany), equipped with a tungsten filament gun, operating at WD 3 mm and an operating voltage of 10 kV.

Dynamic Light Scattering

The solution of **3** at 10 μM concentration was prepared in HPLC water and sonicated for 10 min. Particle size distribution of **3** was measured using dynamic light scattering (DLS) analyzer at a wavelength 657 nm, with Delsa Nano C Particle analyzer (Beckman Coulter, Brea, CA, USA) and at 25 °C.

Cell Assays

Materials and methods

3-(4, 5-Dimethylthiazol-2-yl)-2, 5-diphenyltetrazolium bromide (MTT), trypsin–EDTA, Dulbecco's modified eagle's medium (DMEM, Gibco® Life Technologies, Bengaluru, India), penicillin–streptomycin antibiotic, bisBenzimide H 33258, and gelatin (from cold water fish skin) were purchased from Sigma-Aldrich (Bengaluru, India) and used without further purification. DMSO was obtained from Merck (Bengaluru, India). Fetal bovine serum and CellMask™ deep red plasma membrane stain was purchased from Gibco® Life Technologies.

Cell lines

HeLa cell (immortal cervical cancer cell line), MCF7 (breast cancer cell line), and H460 (lung cancer cell line), were purchased from National Center for Cell Sciences, Pune, India. It is a national repository of cell lines in India. *In vitro* studies were performed to assess the biocompatibility of **3**.

In vitro cell viability/cytotoxicity studies

Cytotoxicity studies were carried out with sterilized solution of **3** at a concentration of 0.25, 0.5, and 1 μM in cell medium to determine if it could be used for biological applications.

3-(4, 5-Dimethylthiazol-2-yl)-2, 5-diphenyltetrazolium bromide assay

In vitro biocompatibility studies of **3** were carried out with HeLa cells by MTT assay [33]. Cells were maintained with Dulbecco's minimum essential medium supplemented with 10% fetal bovine serum in a humid incubator (37 °C and 5% CO_2). Cells (10^4 cells/well) were plated onto 96-well glass-bottom tissue culture plates at an initial confluence of 70%. After 8 h, **3** was added to a final concentration of 0.25, 0.5, and 1 μM, and the wells including the control wells (i.e. only cells) were incubated for ~17 h at 37 °C, in 5% CO_2 humidified incubator followed by removal of media. MTT in DMEM medium (0.5 mg/ml) was prepared and stored in dark environment. After discarding the old media, 200 μl of freshly prepared MTT solution was added to each of the cell-containing wells followed by incubation for 4–5 h. After incubation, basal DMEM (having MTT) was removed, and 200 μl of DMSO was added. The viability of cells was determined by measuring their absorbance at 570 nm. The optical density of absorbance is directly proportional to the number of live cells. All *in vitro* cytotoxicity experiments were performed in quintuplicate, and the best three were taken to quantitate.

Cell uptake studies

Cells (10^4 cells/well) were seeded on a sterilized glass cover slip (13 mm, 0.2% gelatin-coated) for 10 h. To study the cellular uptake of **3** by confocal laser scanning microscopy, a solution

of **3** (1 μM) was added to the cell culture media, which was incubated for ~17 h at 37 °C with 5% CO_2 humidified incubator. After, incubation cells were washed thrice with phosphate buffered saline (PBS) buffer and fixed with 4% formaldehyde solution for 20 min. After washing, cells were stained with deep red plasma membrane dye and washed again with PBS buffer. Coverslips were then mounted on slides coated with buffered mounting medium to prevent fading and drying. Samples were observed under confocal laser scanning microscope (CLSM, Leica SP5, Wetzlar, Germany).

Flow cytometry data

HeLa cells (10^4 cells/well) were grown as described previously, and the cells were incubated with **3** (10 μM in sterilized water, 1 ml) for 17 h. After the incubation, cells were washed with PBS buffer (pH 7.4) and trypsinized by using 0.25% trypsin–EDTA. The cells were then resuspended in PBS (pH 7.4) and analyzed by flow cytometry. The experiments were carried out in triplicate.

For elucidation of the mechanism of particles of **3** in the present work, different cell lines (MCF7, HeLa, and H460) were preincubated for 1 h with inhibitors of endocytosis and micropinocytosis such as filipin III, chlorpromazine, cytochalasin-D, rottlerin, nocodazole, and genistein, followed by incubation with **3** for 17 h afterwards. After exposure of cells to **3**, the cells were trypsinized by using 0.25% trypsin–EDTA after PBS (pH 7.4) wash. The cells were suspended in PBS (pH 7.4) and analyzed by flow cytometry. The experiments were carried out in triplicate.

Result and Discussions

We designed and synthesized conjugates **3** and **4** from FA and diphenylalanine dipeptide using a standard protocol involving DCC coupling method (Scheme 2). Conjugates **3** and **4** were characterized with the help of spectral techniques and their purity established. A number of concentration ranges were assessed for solution-phase self-assembly study of **3**, under aqueous conditions. After some experimentation, with respect to solubility characteristics, we recorded SEM micrographs at two different concentrations (1 mM and 10 μM). Worm-like, short self-assembled structures were observed (Figure 1(A,B)), which clearly looked very different from the well-established nanotubular morphology observed for diphenylalanine dipeptide alone. This suggests that not only self-assembly of **3** is concentration dependent but the two components influence and modulate self-assembly behavior of the conjugate. Difference observed with the present conjugate may be ascribed to the number of molecules in stacked orientation and to the extent of solvent intervention during H-bond formation.

Dynamic light scattering experiments were performed with 10 μM aqueous solutions of sample **3**, revealing the hydrodynamic cross section in the range of ~550–700 nm (Figure 1(C)). Self-assembly study for **4** also revealed the formation of similar worm-like morphologies under aqueous conditions (Figure 1(D)). Notably, both **3** and **4** showed similar gross morphological features, despite the presence of additional hydrogen-bonding sites in **4**.

Folic acid units are proposed to exist as tetramers (Figure 2(A,B)). Tetrameric ensembles of FA are known to self-assemble, with the help of eight intermolecular hydrogen bonds, to form stacked, columnar structures [15]. Incidentally, diphenylalanine dipeptide is also known to form hollow nanotubes because of π–π stacking and H-bonding interactions. Thus, it could be surmised that a combination of noncovalent interactions in **3** and **4** governs final morphologies of these conjugates. A proposed model for various interactions is given in Figure 2.

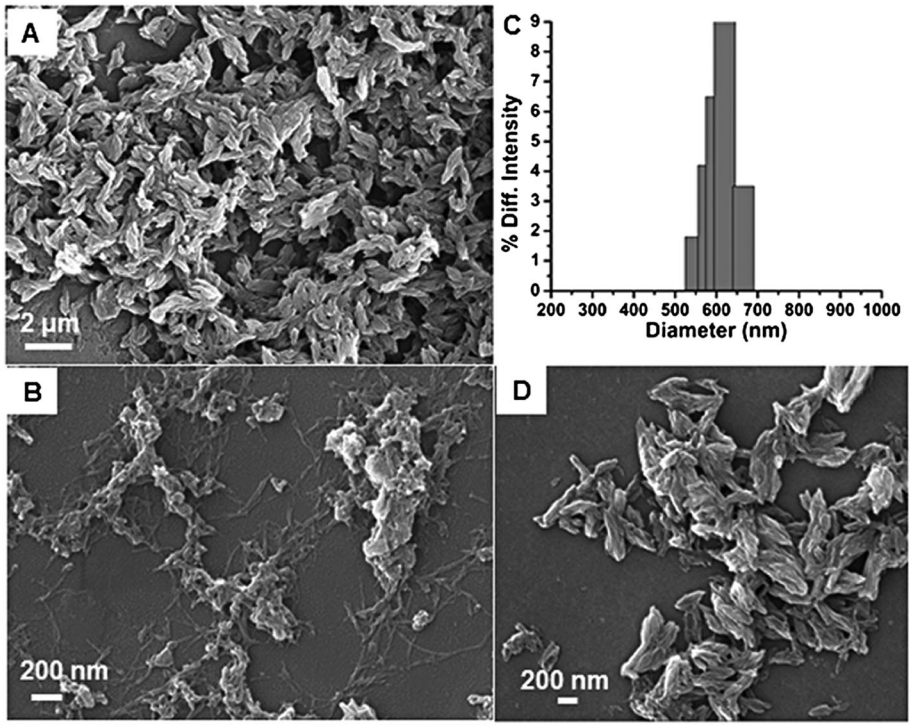

Figure 1. Microscopy analysis of **3** on Si(100) wafer in water: (A) 1 mM; (B) 10 μM concentration; (C) dynamic light scattering analysis of **3** at 10 μM; and (D) scanning electron microscopy image of **4** at 10 μM.

Journal of PeptideScience

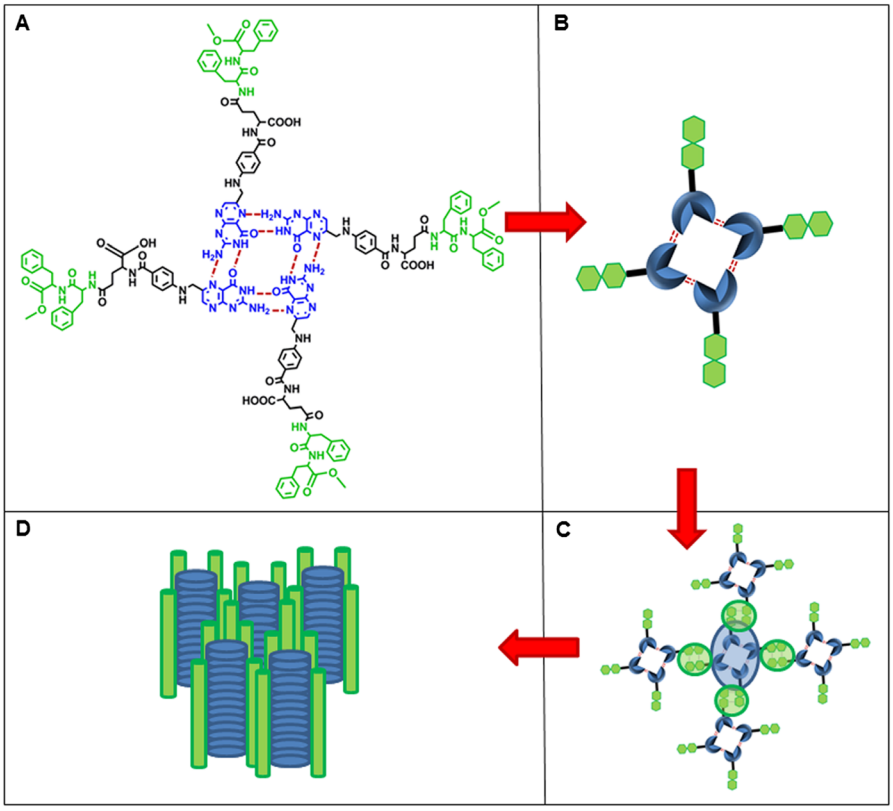

Figure 2. Hypothetical model showing folic acid-guided self-assembly for **3** and **4**: (A) proposed core tetramer of folic acid units; (B) model tetramers formed by the Phe–Phe conjugates; (C) proposed interactions between various tetramer units and Phe–Phe units; and (D) stacked, columnar self-assembled structures.

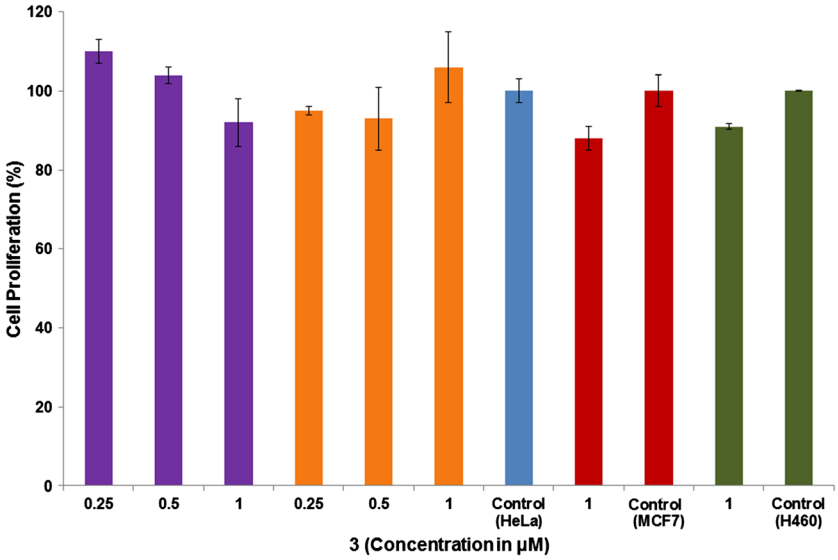

Figure 3. *In vitro* biocompatibility assay of **3** at different concentrations in HeLa cells (17 h incubation) [purple bars (sample in medium) and orange bars (sample in HPLC water, diluted by medium)] and MCF7 (red bars, sample in HPLC water) and H460 (green bars, sample in HPLC water) cancer cells.

Further experiments were carried out with **3** because of solubility constraints of conjugate across microscopy and cell culture studies. As the premise of this study was to check the effect of FA conjugation in dipeptide self-assembly uptake, we decided to first work with three concentrations (0.25, 0.5, and 1 μM) to find out the cytotoxicity properties of **3**.

3-(4, 5-Dimethylthiazol-2-Yl)-2, 5-Diphenyltetrazolium Bromide Assay Study

In vitro cytotoxicity of **3** was studied on HeLa cells by MTT assay using three different concentration ranges (0.25, 0.5, and 1 μM), to investigate the effect of these particles on cell viability. Samples

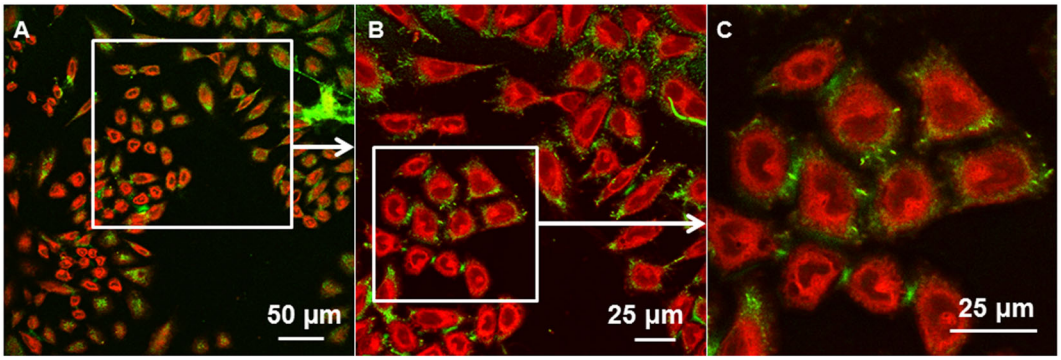

Figure 4. (A) Confocal microscopy images showing uptake of **3** in HeLa cells; (B,C) magnified view. HeLa cells were stained with deep red plasma membrane dye, which exhibits red emission (λem = 633 nm); green emission (λem = 488 nm) in A–C is ascribed to **3**.

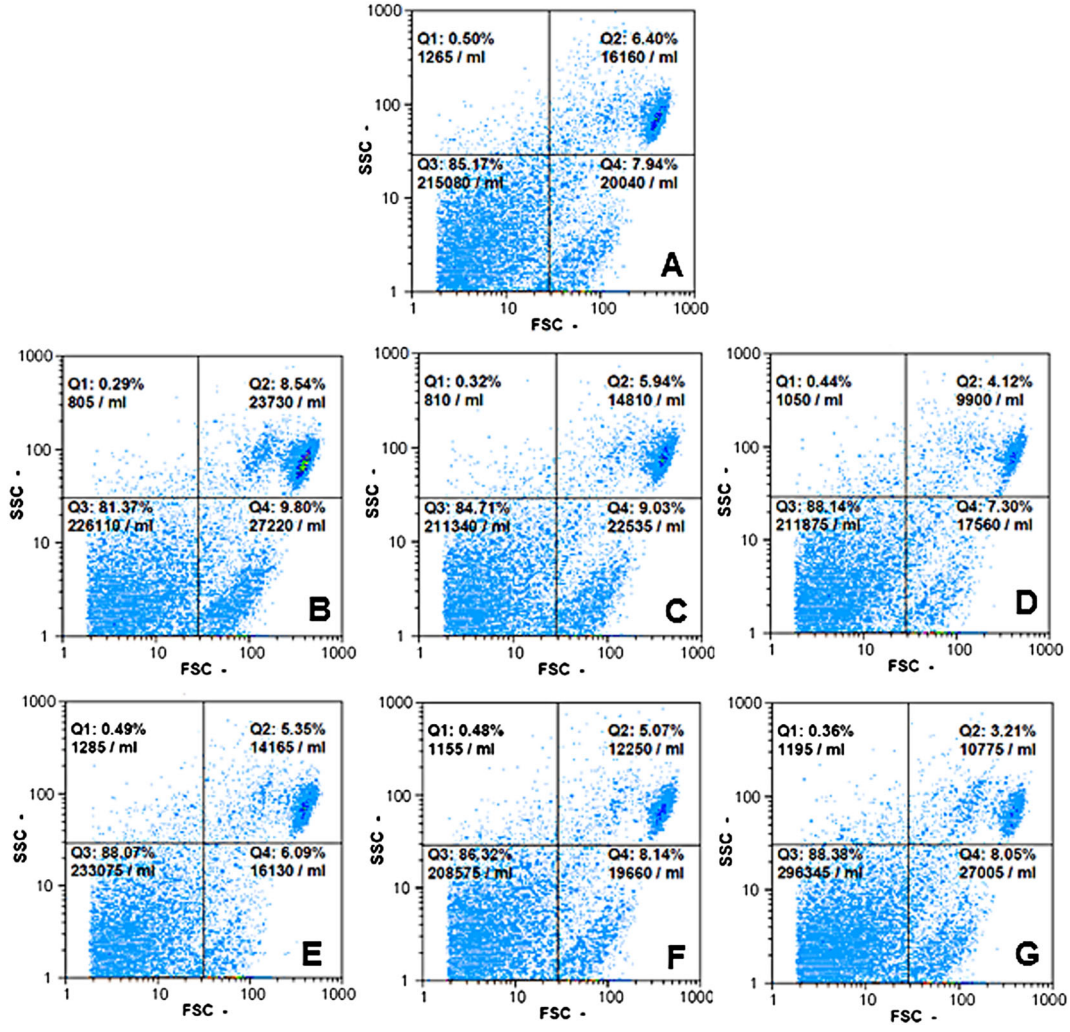

Figure 5. Flow cytometry assay of HeLa cells preincubated for 1 h with endocytic inhibitors: (A) no inhibitor; (B) filipin III; (C) genistein; (D) nocodazole; (E) cytochalasin-D; (F) chlorpromazine; and (G) rottlerin (highlighted Q2). SSC, side scatter; FSC, forward scatter.

were prepared in DMEM by two methods: (i) powder sample was dissolved in medium and (ii) solution was prepared in HPLC grade water, followed by dilution with DMEM. It was observed that cell proliferation percentages for **3** were nearly similar to that of nontreated cell control, i.e. they are biocompatible (Figure 3, purple and orange bars). Because both sample preparations showed non-toxic behavior, we opted for sample prepared in HPLC water, followed by dilution, for further studies. MTT assay was also carried out with MCF7 and H460 cancer cell lines, which confirmed noncytotoxic nature of **3** (Figure 3, red and green bars).

Journal of PeptideScience

Cellular Uptake Study

Conjugate **3** was designed in such a way so that it could interact with FRs in cancer cells and achieve cellular entry [34,35]. Notably, **3** also exhibits fluorescence emission making it convenient to be monitored by fluorescence microscopy methods. Nontoxic and biocompatible nature of conjugate **3** motivated us to further investigate its uptake and internalization in HeLa cells. These cells were incubated with **3** (1 μM) for 17 h and observed under confocal microscope, suggesting uptake of **3** by HeLa cells (Figure 4).

Elucidation of Uptake Mechanism

Flow cytometry was used to determine the probable uptake mechanism of **3** (10 μM) in cancer cells. This technique offers simultaneous measurement and analysis of multiple physical characteristics of single cells, as they pass through a beam of light in a fluid stream. It is commonly used for cell counting and sorting, biomarker detection, and in clinical studies. Of the many measurable properties such as relative size, relative granularity, and relative fluorescence intensity, we decided to use the latter for our experiments. In these analyses, optical information known as forward scatter (FSC) and side scatter (SSC) were collected, where FSC essentially provides information correlating cell size, while SSC provides information on cell granularity. FSC *versus* SSC plot is a basic method of visualizing flow cytometric data, and the upper-right quadrant (i.e. Q2), provides information about cells positive for **3**, whereas cells negative for **3** are found in the bottom-left quadrant (Q3). For this purpose, a positive control experiment was carried out with HeLa cells (Figure 5(A)), H460 (Figure S1), and MCF7 cell lines (Figure S2), in the presence of **3**, which suggested that cells internalized **3** and exhibited an increase in cell size.

Uptake mechanism of **3** by various cancer cells was probed by different inhibitors, such as filipin III (1 μg/ml), chlorpromazine (5 μg/100 μl), cytochalasin-D (5 μM), rottlerin (25 μg/ml), nocodazole (20 μM), and genistein (100 μM), which selectively interfere with various endocytic pathways. Filipin III and genistein are known to inhibit caveolae-mediated endocytosis, chloropromazine inhibits clathrin-mediated endocytosis, and rottlerin is a selective inhibitor of macropinocytosis, while cytochalasin-D inhibits actin polymerization, thus inhibiting both phagocytosis and macropinocytosis.

Uptake of **3** in HeLa (Figure 5) and H460 cells (lung cancer) (Figure S1), in the presence of all inhibitors, was analyzed by flow cytometry. In both cell lines, rottlerin leads to maximum decrease in the percentage of cell population (Q2) with internalized particles of **3**, as compared with positive control, which showed partial-to-complete inhibition. This suggested that internalization perhaps occurs through a macropinocytosis-mediated pathway for HeLa and H460 cells. However, in case of MCF7 cell line, chlorpromazine and nocodazole inhibited internalization of **3**, which suggests a probable role of clathrin-mediated endocytosis in the uptake process (Figure S2). Thus, it appears that different cell lines used different endocytic pathways for the transport of **3** particles [36–39]. It must be mentioned that there are numerous reports for folate conjugates following multiple pathways for cellular entry, thus suggesting that entry via FR is not a unique pathway for cell uptake [34,40] and monovalency or multivalency of folate conjugates has little effect on the rate of cell internalization, knowing that multivalent folate conjugates are possibly taken up via different endocytic pathways [41].

Conclusion

Folic acid diphenylalanine derivatives were synthesized and studied for their self-assembled behavior. New morphological structures were obtained compared with FA and diphenylalanine peptide alone. Further, MTT assay showed biocompatible nature and stable behavior of these derivatives. Conjugate **3** could be used as potential delivery vehicle, with further modifications to optimize required solubility properties, as the cellular uptake studies and uptake mechanism studies confirmed internalization of **3** in three different cancer cell lines. Uptake of **3** in HeLa and H460 was ascribed to macropinocytosis-mediated pathway based on rottlerin, suggesting a probable role of clathrin-mediated endocytosis in cell internalization. We intend to use **3** and related vehicles for selective delivery of bioactives in cancer cells.

Acknowledgements

We thank DST Thematic Unit of Excellence in Soft Nanofabrication, IIT Kanpur, for FE-SEM and DLS. We thank Prof. P. Sinha, BSBE, IIT Kanpur, for allowing us to use confocal microscope in his laboratory. G. K. thanks IIT Kanpur and UGC, India, for financial support. This work is supported by an Outstanding Investigator Award to S. V. from DAE-SRC, Department of Atomic Energy, India, J. C. Bose National Fellowship, DST, India, and by a MHRD-supported Centre for Excellence in Chemical Biology, IIT Kanpur.

References

1 Kamaly N, Kalber T, Thanou M, Bell JD Miller AD. Folate receptor targeted bimodal liposomes for tumor magnetic resonance imaging. *Bioconj Chem* 2009; **20**: 648–655.
2 Xia W, Low PS. Folate-targeted therapies for cancer. *J Med Chem* 2010; **53**: 6811–6824.
3 Chen C, Jiyuan K, Edward ZX, Wei Y, Joseph SB, Jun L, Eu-Leong Y, Eric XH Karsten M. Structural basis for molecular recognition of folic acid by folate receptors. *Nature* 2013; **500**: 486–489.
4 Sudimack J, Lee RJ. Targeted drug delivery via the folate receptor. *Adv Drug Deliv Rev* 2000; **41**: 147–162.
5 Paulos CM, Reddy JA, Leamon CP, Turk MJ, Low PS. Ligand binding and kinetics of folate receptor recycling *in vivo*: impact on receptor-mediated drug delivery. *Mol Pharmacol* 2004; **66**: 1406−1414.
6 Wang S, Low PS. Folate-mediated targeting of antineoplastic drugs, imaging agents, and nucleic acids to cancer cells. *J Control Release* 1998; **53**: 39−48.
7 Xiaofeng W, Wenlie L, Na M, Fang L, Zhenyu L, Longhua G, Bin Q Guonan C. Sensitive fluorescence biosensor for folate receptor based on terminal protection of small-molecule-linked DNA. *Chem Commun* 2012; **48**: 6184–6186.
8 Cooper MA. Optical biosensors in drug discovery. *Nat Rev Drug Discov* 2002; **1**: 515–528.
9 Nien-Chu F, Fong-Yu C, Ja-an AH Chen-Sheng Y. Photocontrolled targeted drug delivery: photocaged biologically active folic acid as a light-responsive tumor-targeting molecule. *Angew Chem Int Ed* 2012; **51**: 8806–8810.
10 Li J, Sausville EA, Klein PJ, Morgenstern D, Leamon CP, Messmann RA, LoRusso P. Clinical pharmacokinetics and exposure-toxicity relationship of a folate-vinca alkaloid conjugate EC145 in cancer patients. *J Clin Pharmacol* 2009; **49**: 1467−1476.
11 Leamon CP, Reddy JA, Vlahov IR, Westrick E, Dawson A, Dorton R, Vetzel M, Santhapuram HK, Wang Y. Preclinical antitumor activity of a novel folate-targeted dual drug conjugate. *Mol Pharm* 2007; **4**: 659−667.
12 Bonazzi S, DeMorais MM, Gottarelli G, Mariani P Spada GP. Self-assembly and liquid crystal formation of folic acid salts. *Angew Chem Int Ed Engl* 1993; **32**: 248–250.
13 Ciuchi F, Nicola GD, Franz H, Gottarelli G, Marisni P, Bassi MGP Spada GP. Self-recognition and self-assembly of folic acid salts. *J Am Chem Soc* 1994; **116**: 7064–7071.

14 Federiconi F, Mattioni M, Baldassarri EJ, Ortore MG Mariani P. How soft are biological helices? A measure of axial and lateral force constants in folate quadruplexes by high-pressure X-ray diffraction. *Eur Biophys J* 2011; **40**: 1225–1235.
15 Xing P, Chu X, Ma M, Li S Hao A. Supramolecular gel from folic acid with multiple responsiveness, rapid self-recovery and orthogonal self-assemblies. *Phys Chem Chem Phys* 2014; **16**: 8346–8359.
16 Thomas A, Shukla A, Sivakumar S Verma S. Assembly, postsynthetic modification and hepatocyte targeting by multiantennary, galactosylated soft structures. *Chem Commun* 2014; **50**: 15752–15755.
17 Kaur G, Alder-Abramovich L, Gazit E Verma S. Ultrastructure of metallopeptide-based soft spherical morphologies. *RSC Adv* 2014. DOI: 10.1039/C4RA10532J.
18 Ghosh S, Alder-Abramovich L, Gazit E Verma S. Spacer driven morphological twist in Phe-Phe dipeptide conjugates. *Tetrahedron* 2013; **69**: 2004–2009.
19 Barman AK, Verma S. Solid state structures and solution phase self-assembly of clicked mannosylated diketopiperazines. *RSC Adv* 2013; **3**: 14691–14700.
20 Mishra NK, Joshi KB Verma S. Inhibition of human and bovine insulin fibril formation by designed peptide conjugates. *Mol Pharm* 2013; **10**: 3903–3912.
21 Barman AK, Chaturbedi A, Subramaniam K Verma S. Imaging C. elegans with thiolated tryptophan-based NIR fluorescent gold nanoclusters. *J Nanopart Res* 2013; **15**: 2083.
22 Modal S, Barman AK Verma S. Peptide-based synthetic design, construction and morphology of soft structures. *Chimia* 2012; **66**: 930–935.
23 Gour N, Braman AK Verma S. Controlling morphology of peptide-based soft structures by covalent modifications. *J Pep Sci* 2012; **18**: 405–412.
24 Barman AK, Verma S. Sunlight mediated disruption of peptide-based soft structures decorated with gold nanoparticles. *Chem Commun* 2010; **46**: 6992–6994.
25 Joshi KB, Verma S. Ditryptophan conjugation triggers conversion of biotin fibers into soft spherical structures. *Angew Chem Int Ed* 2008; **47**: 2860–2863.
26 Singh P, Venkatesh V, Nagapradeep N, Verma S Bianco A. G-quartet type self-assembly of guanine-functionalized singled walled carbon nanotubes. *Nanoscale* 2012; **4**: 1972–1974.
27 Castillo JJ, Rindzevicius T, Wu K, Schmidt MS, Janik KA, Boisen A, Svendsen W, Rozlosnik N Castillo-León J. Synthesis and characterization of covalent diphenylalanine nanotube-folic acid conjugates. *J Nanopart Res* 2014; **16**: 2525.
28 Reches M, Gazit E. Casting metal nanowires within discrete self-assembled peptide nanotubes. *Science* 2003; **300**: 625–627.
29 Adler-Abramovich L, Aronov D, Beker P, Yevnin M, Stempler S, Buzhansky L, Rosenman G Gazit E. Self-assembled arrays of peptide nanotubes by vapour deposition. *Nat Nanotechnol* 2009; **4**: 849–854.
30 Santhanamoorthi N, Kolandaivel P, Adler-Abramovich L, Gazit E, Filipek S, Viswanathan S, Strzelczyk A Renugopalakrishnan V. Diphenylalanine peptide nanotube: charge transport, band gap and its relevance to potential biomedical applications. *Adv Mat Lett* 2011; **2**: 100–105.
31 Yan X, Zhu P Li J. Self-assembly and application of diphenylalanine-based nanostructures. *Chem Soc Rev* 2010; **39**: 1877–1890.
32 Adler-Abramovich L, Reches M, Sedman VL, Allen S, Tendler SJB Gazit E. Thermal and chemical stability of diphenylalanine peptide nanotubes: implications for nanotechnological applications. *Langmuir* 2006; **22**: 1313–1320.
33 Mosmann T. Pages rapid colorimetric assay for cellular growth and survival: application to proliferation and cytotoxicity assays. *J Immunol Methods* 1983; **65**: 55–63.
34 Dong S, Cho HJ, Lee YW, Roman M. Synthesis and cellular uptake of folic acid-conjugated cellulose nanocrystals for cancer targeting. *Biomacromolecules* 2014; **15**: 1560−1567.
35 Yameen B, Choi WI, Vilos C, Swami A, Shi J Farokhzad OC. Insight into nanoparticle cellular uptake and intracellular targeting. *J Control Release* 2014; **190**: 485–499.
36 Vercauteren D, Vandenbroucke RE, Jones AT, Rejman J, Demeester J, Smedt SCD, Sanders NN Braeckmans K. The use of inhibitors to study endocytic pathways of gene carriers: optimization and pitfalls. *Mol Ther* 2010; **18**: 561–569.
37 Sarkar K, Kruhlak MJ, Erlandsen SL Shaw S. Selective inhibition by rottlerin of macropinocytosis in monocyte-derived dendritic cells. *Immunology* 2005; **116**: 513–524.
38 Sami H, Maparu AK, Kumar A Sivakumar S. Generic delivery of payload of nanoparticles intracellularly via hybrid polymer capsules for bioimaging applications. *PLoS One* 2012; **7**: e36195.
39 Schnitzer JE, Oh P, Pinney E Allard J. Filipin-sensitive caveolae-mediated transport in endothelium: reduced transcytosis, scavenger endocytosis, and capillary permeability of select macromolecules. *J Cell Biol* 1994; **127**: 1217.
40 Li YL, Cuong NV Hsieh MF. Endocytosis pathways of the folate tethered star-shaped PEG-PCL micelles in cancer cell lines. *Polymers* 2014; **6**: 634–650.
41 Bandara NA, Hansen MJ Low PS. Effect of receptor occupancy on folate receptor internalization. *Mol Pharm* 2014; **11**: 1007–1013.

Supporting Information

Additional supporting information may be found in the online version of this article at the publisher's web site.